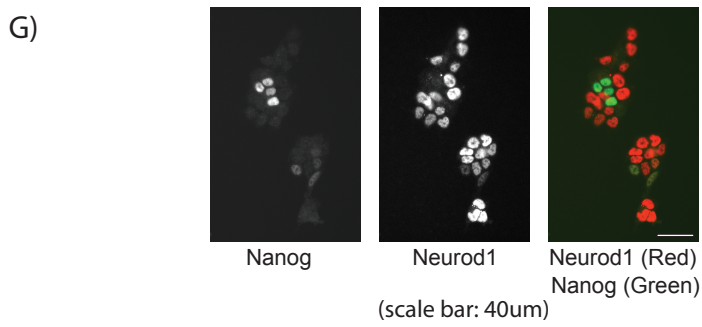
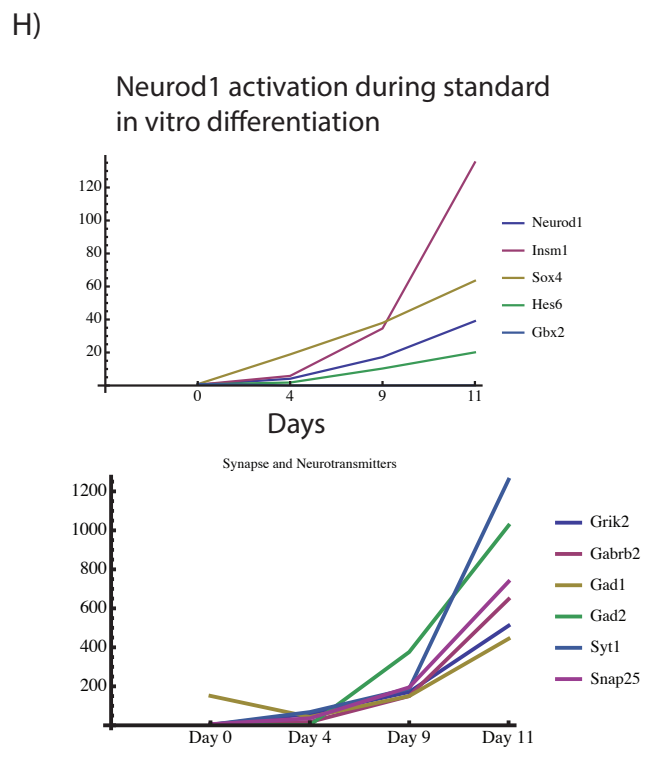
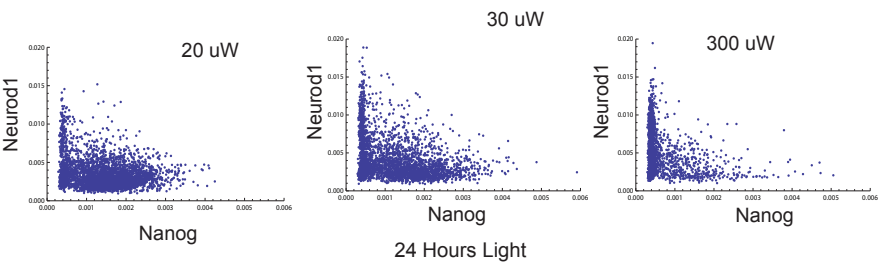
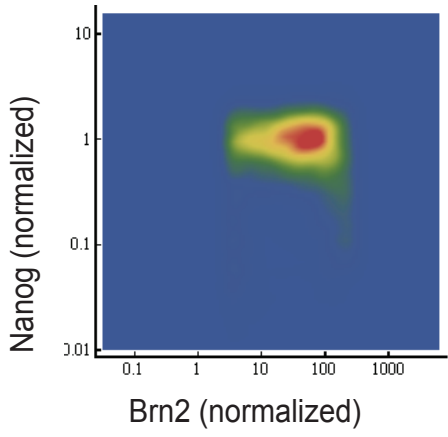


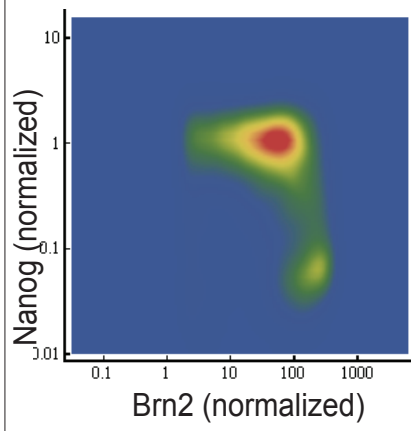
F) Neurod1 Activation in Nanog-off cells



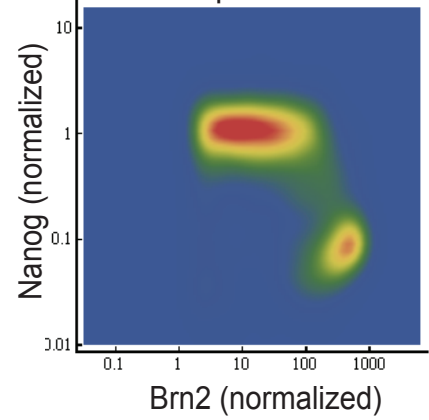
A) 24 hours (10uW)



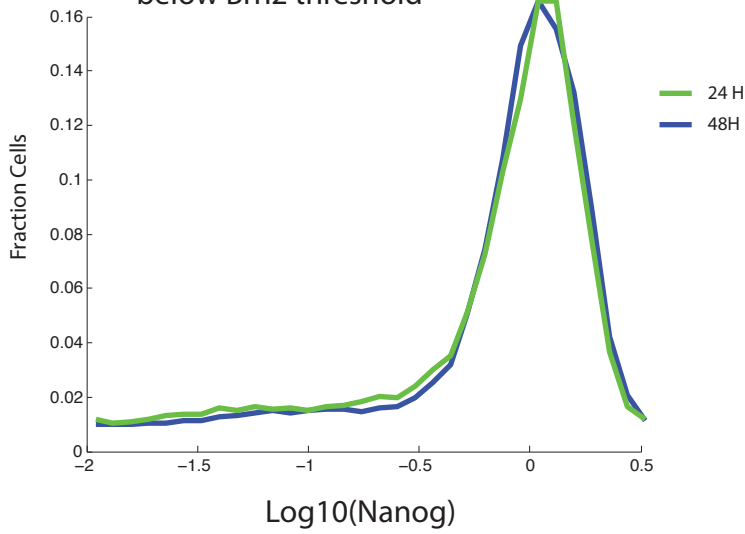
48 hours (10uW)



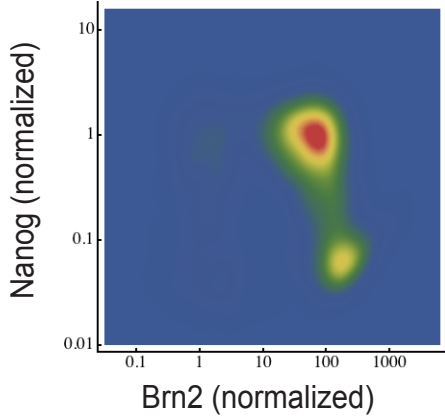
48 hours uniform sampling of Brn2 expression bins



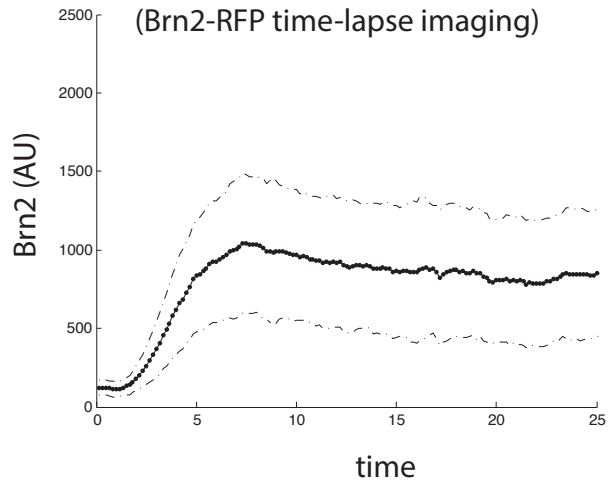
B) Nanog-GFP expression distribution for cells sampled below Brn2 threshold



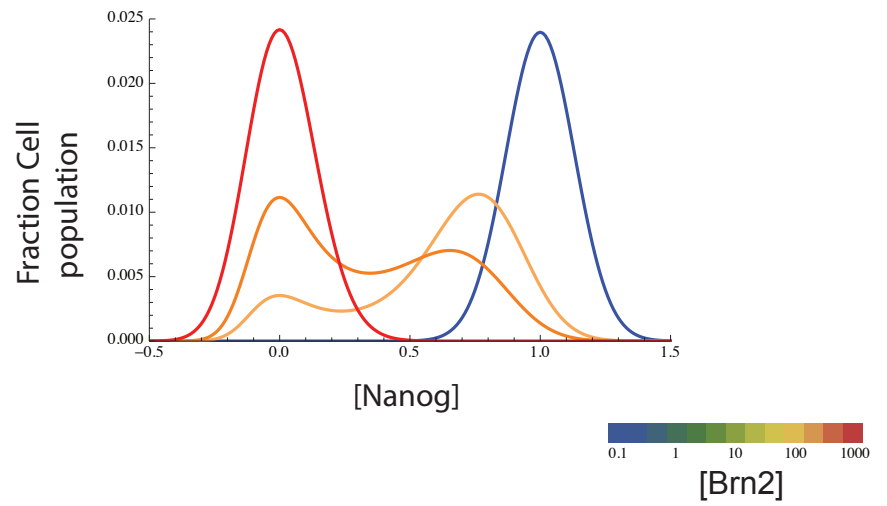
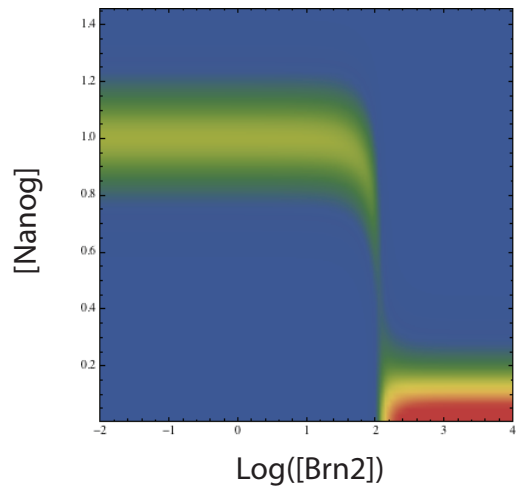
C) 1 hr light pulses 6 hr spacing (300uW Light)



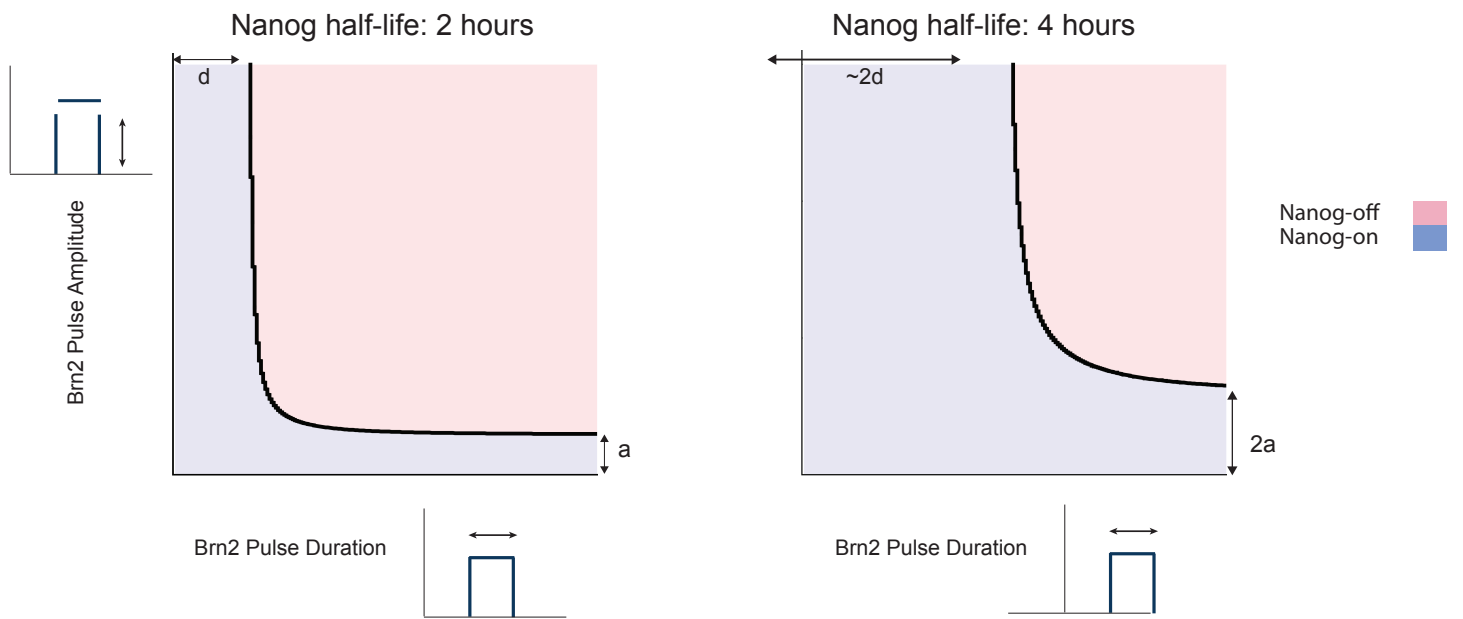
1 hr light pulses 6 hr spacing (Brn2-RFP time-lapse imaging)



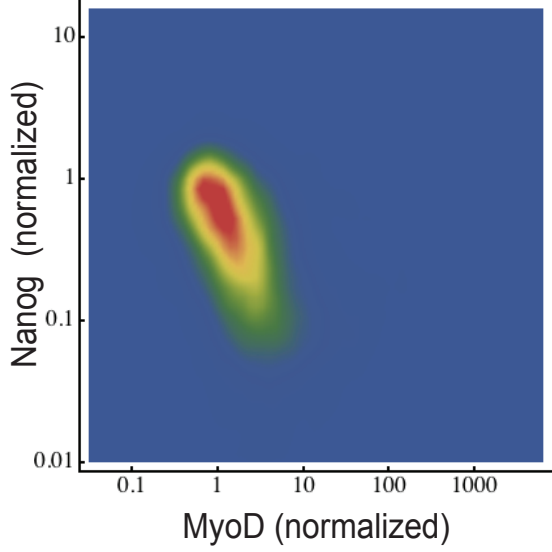
A)



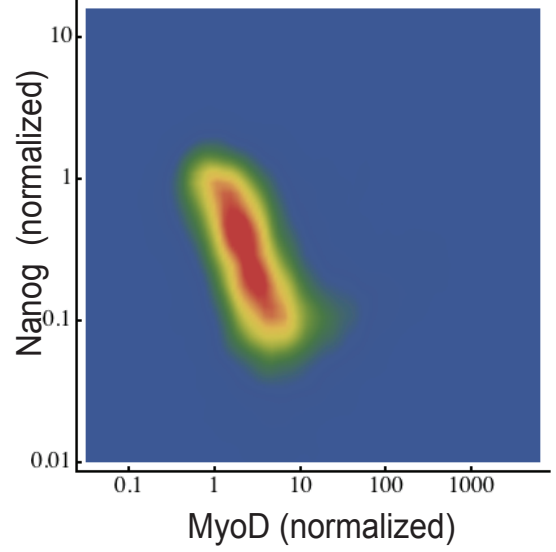
B)



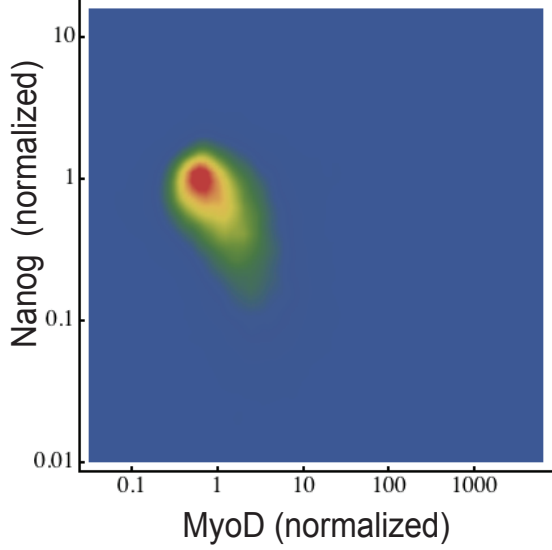
A) 15uW Light excitation 24 hours



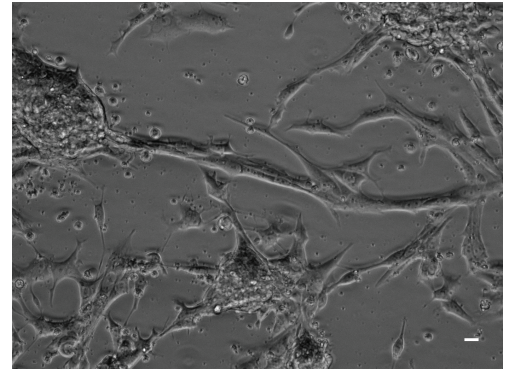
B) 25uW Light excitation 24 hours



C) 4uW Light excitation 24 hours

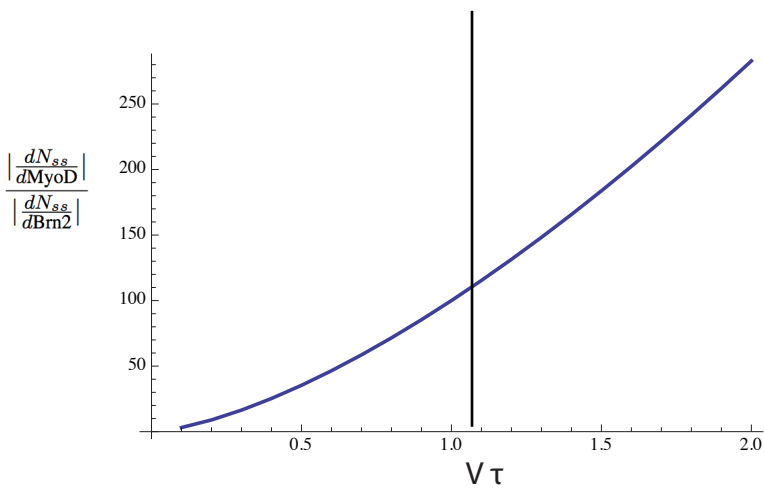


D) MyoD induced ES cells
(72 Hours, 300uW)



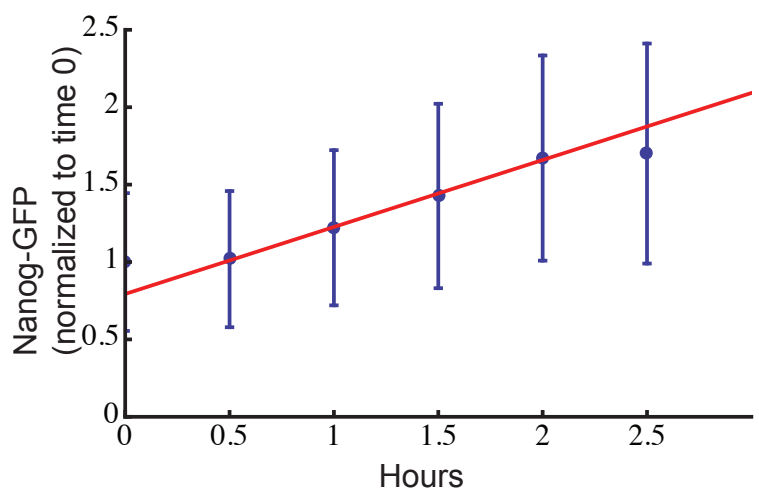
Phase contrast (40um scale bar)

E)



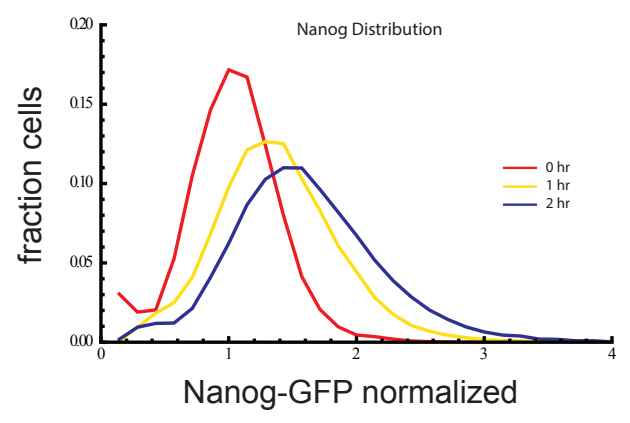
— 1.05 is magnitude of $V \tau$
used in our model

A)



slope = .45 / hour

B)



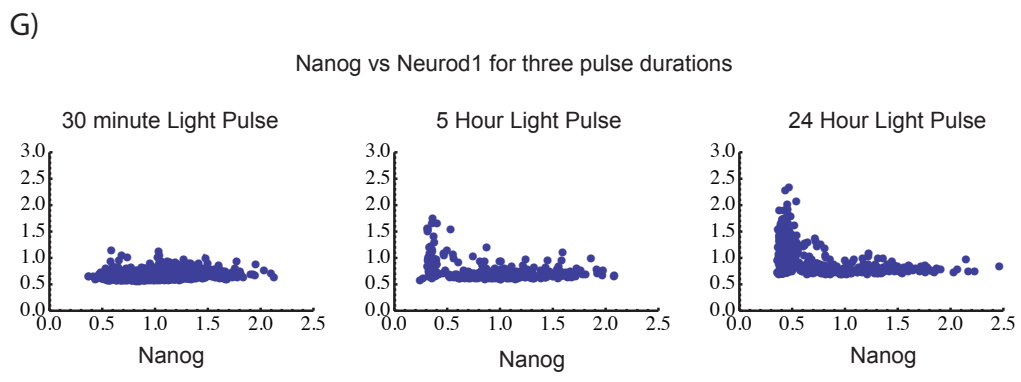
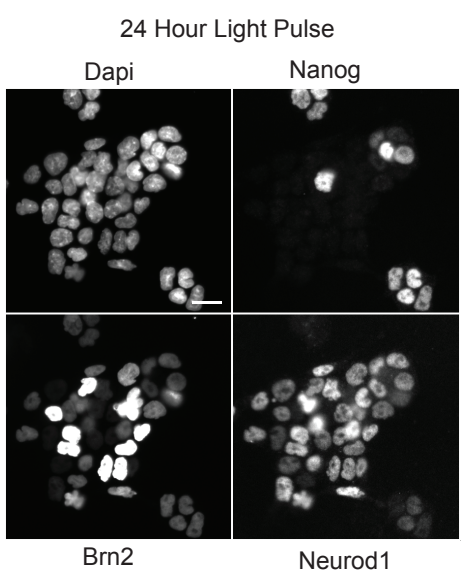
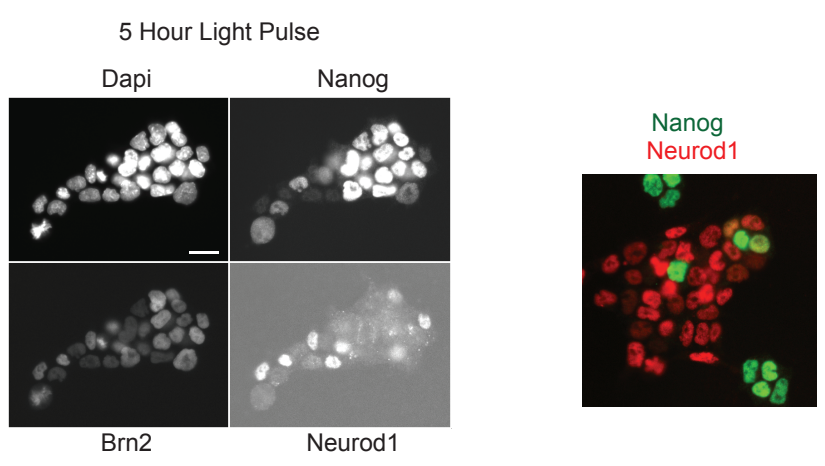
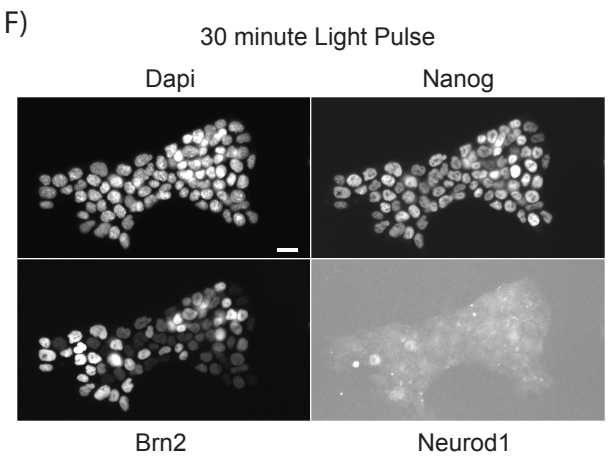
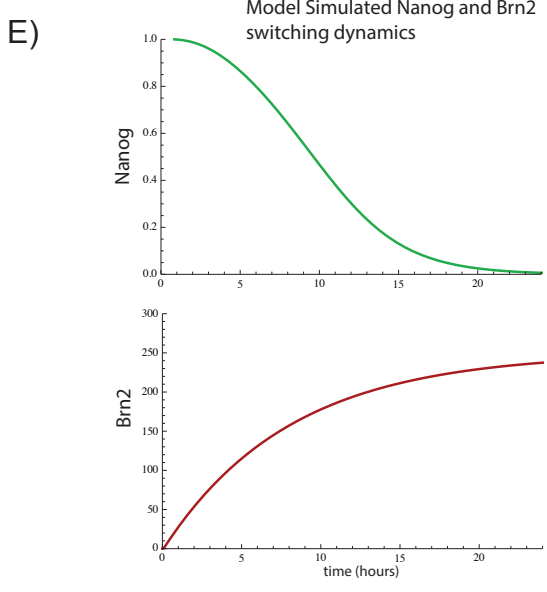
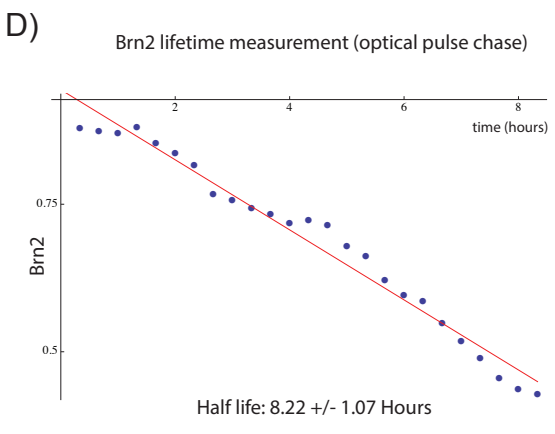
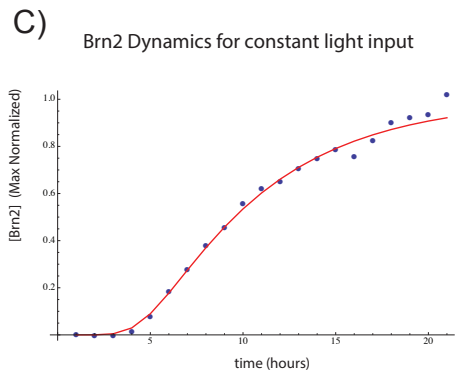
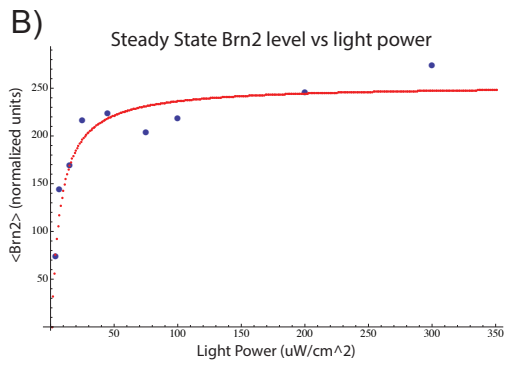
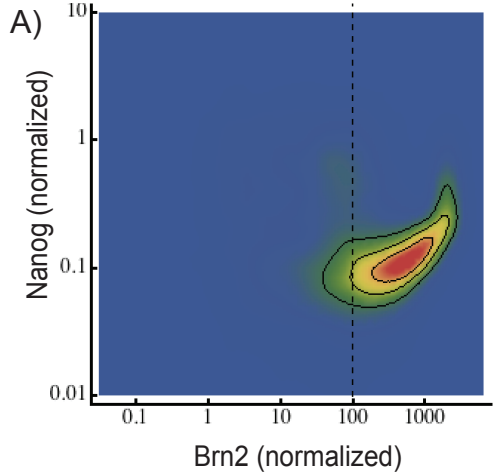


Table S1

| Name | Sequences |
|----------------|--|
| sgRNA F | ggagaaccacctgttggcgtaagtctcatatttcaccgtttaagagctatgctggaacagca |
| sgRNA R | ctagtactcgagaaaaaagcaccgactcgggtgccac |
| 5' HR F | aggggttccgcgcacattccccgaaaagtgccacctgacaagttgctgtaatgtaacacaatgagactgact |
| 5' HR R | tcacactcctccacctgagccacctccagagcctccacctatttcacctggtggagtcacagag |
| 3' HR F | tgagacttacgcaacatctgggcttaaag |
| 3' HR R | tagccctcctctgggtgattg |
| eGFP F | ggtggaggctctggaggtggctcaggtggagggagtgtagcaagggcgaggagc |
| eGFP R | ctttgccctgactttaagcccagatgttgcgtaagtctcactgtacagctcgtccatgccg |
| Vector F | gggtggaagagattccaccaatcaccaggagtggggctaaaacggctcctccagcttggtg |
| Vector R | attagcaagtcagctcattgtgttacattacagcaactgtcaggtggcacttttcgggga |
| Primer set 1 F | attcttctaccagtcccaaaaaagctctc |
| Primer set 1 R | cttgtagctcgtccatgccg |
| Primer set 2 F | gaagagcatttccccagcac |
| Primer set 2 R | agtccagctggcatcggttca |

SI Figure Legends:

Figure SI 1: Construction of light inducible Brn2 expression system. Generation of Nanog-GFP knock-in reporter cell line through Cas9 mediated homologous recombination, related to Figure 1

A) Design of gene expression vectors for optogenetic Brn2 induction. The GAVPO protein is a synthetic transcription factor that homodimerizes to drive the GAL4-UAS in the presence of blue light (Wang, Nature Methods, 2012). We engineered a PiggyBac expression vector with puromycin resistance that drives that GAVPO protein from the eF1alpha promoter for constitutive expression in ES cells. In our system, a second expression vector contains the four copies of the GAL4-UAS upstream of the gene of interest, Brn2. Brn2 is additionally fused to TAGRFPT2 separated by a 3x glycine serine linker. **B)** Distribution of Brn2-RFP in the dark (blue) and following 24 hours of light activation ($300\text{uW}/\text{cm}^2$) (pink). Brn2-RFP level is shown normalized to the mean fluorescence intensity of the dark distribution. **C)** Phase contrast and fluorescence images of Brn2-GAVPO ES cells in the dark and **D)** following 24 hours of light induction. In the dark, cell colonies remain round and do not contain nuclear RFP. Following light activation, colonies are flat and contain bright nuclear RFP signal. (20um scale bars) **E)** IF staining of Brn2-GAVPO ES cell colony in the dark showing that cells stain positive for Nanog prior to light induction and negative for Nanog after 24 hours 300uW blue light (scale bar, 20 um). **F)** Brn2-GAVPO transfected with a cytoplasmic GFP following 72 hours of light exposure. Colonies have started to form a dense network of interconnected projections. (scale bar, 40um) **G)** Brn2 activation and decay as a function of time following a one hour light pulse at 300uW as measured by FACS. The graph shows the mean as well as the top and bottom quintiles for a population of $>30,000$ cells at each time point. The plot has been normalized to the mean Brn2-RFP level in a population of cells exposed to constant light for 24 hours. **H)** Schematic of strategy to generate a Nanog-EGFP knock-in allele using CAS9. The stop codon of Nanog is labeled in red. The sgRNA coding sequence is capitalized and underlined. HA-L (2 kb) and HA-R (3 kb) represent the homologous arms of the donor vector. **I)** Detection of the EGFP insertion in ES cells. Primer set #1: an external forward primer specific for an upstream sequence outside of homologous arms and an internal reverse primer specific for EGFP. Primer set #2: a pair of internal forward and reverse primers targeting a region > 1000 nt up- and down-stream of the EGFP. 1) Wild-type ES cells. 2) Monoallelic EGFP insertion ES cells. 3 and 4) Biallelic EGFP insertion ES cells. **J)** Top: Representative image of Nanog-EGFP expression in Nanog-EGFP biallelic ES cells. **Bottom:** Representative image of Nanog-EGFP expression in differentiated biallelic Nanog-EGFP ES cells. ES cells are differentiated for 3 days under DMEM medium with 10% FBS. Cells in C and D acquired using same imaging settings. **K)** Nanog distributions for cells maintained in differentiation and non-differentiation media from image analysis. Plot shows down regulation of Nanog following 24 hours of forward differentiation. **L)** Scatter plots of Nanog and Brn2 collected using immunofluorescence staining for Nanog and Brn2-RFP to confirm measurements with knock-in cell line. For each plot, a panel of IF images were collected and automated image analysis was performed using DAPI co-stain to detect > 500 cells. Scatter plots show that cell population shifts from being entirely Nanog-on when exposed to $1\text{uW}/\text{cm}^2$ of light for

24 hours (Top) to having an “L” shape where Nanog and Brn2 are mutually exclusive after 24 hour exposure at 300uW/cm² (Bottom). Data is not as quantitative as FACS data due to image segmentation but provides qualitative confirmation of data collected with Nanog-GFP cell line.

SI Movie 1, related to Figure 1: Time lapse imaging of Brn2-TAGRFPT induction. Cells exposed to continuous 300uW/cm² blue light. Images captured every 20 minutes for 20 hours. TAGRFPT fluorescence is localized to the cell nucleus.

Figure SI 2: RNA-seq data and FACS analysis reveal Brn2 activation of a neural gene expression program that includes Neurod1 Cell death and photobleaching controls, related to Figure 1. **A)** Phase contrast and dead cell stain images of cells following 48 hours of light activation at 300uW. Dead-cell stain identifies a small patch of cells that stain positive. For comparison, Invitrogen dead cell stain and phase contrast images of cells exposed to 1.2mW of light for 72 hours to induce strong cell death. Scale bar (20um in both sets of images). **B)** FACS quantification of cell death with 7AAD at (dark), 24 and 48 hours of Brn2 activation with 300uW. For each sample, quantification was done in >30,000 cells. Bar graph indicates the number of “dead-cells” as extracted through quantification in the bulge of the 7AAD histogram. **C)** FACS quantification of Nanog-GFP levels in cells lacking the Brn2 inducible construct (blue and purple curves). Yellow curve shows control cell population with Brn2 inducible construct. Histograms show that Nanog-GFP levels are indistinguishable in cells exposed to 300uW blue light vs in the dark. Bottom plot shows mean and standard deviation of Nanog-GFP in three cell populations. This data is consistent with the published literature showing minimal bleaching at the light powers used for optical induction in our experiments. **D)** Fold change over time of the top activated/repressed transcription factors from RNA-seq. **E)** The distribution of Neurod1 expression as measured by immunostaining of Neurod1 and FACS at 0, 14, and 24 hours of Brn2 induction. The shape of the Neurod1 distribution shifts to the right following activation. At 14 hours two cell populations appear, and by 24 hours the distribution function is clearly separated. Imaging (as in Figure 1) showed the absence of nuclear Neurod1 for transient Brn2 induction and its nuclear presence following light induction of 24 hours at high power. **F)** We verified by immunofluorescence that Neurod1 is expressed in Nanog-off (differentiated) cells across a large range of light powers suggesting that the switch from the Nanog-on (pluripotent) to Nanog-off (differentiated) state precedes neural differentiation. Brn2-ES cells induced with the indicated light power (power is in uW but distance unit omitted for clarity) and stained for Neurod1 using IF and alexa 647. Microscopy and automated image analysis were used to segment > 500 cells at each light power and measure Nanog and Neurod1 intensities in each cell. In the scatter plots, each dot represents a single cell. Nanog and Neurod1 are shown in arbitrary fluorescence units, which are identical across plots. Scatter plots contain an “L” shape that becomes pronounced at high light powers. This shape indicates that Neurod1 and Nanog are expressed in mutually exclusive cell populations; Neurod1 is activated in cells that down-regulated Nanog. **G)** IF images of Brn2-GAVPO ES cells following 24 hours of light exposure. Neurod1 present (Red) and mutually exclusive with Nanog-positive cells (Green) (40 um scale bar). **H)** RNA-seq shows that Neurod1, Insm1, Sox4, Hes6, and Gbx2 (top left) – genes that are activated by

Brn2-GAVPO within 24 hours become activated at approximately 9 days in this protocol. A series of neural markers for synapse function (top, left), Electrical activity (top, right) and neural connectivity and migration (bottom, right) are shown to provide context for the terminal state of the neurons from in vitro differentiation experiment.

SI Movie 2, related to Figure 1: Phase contrast time-lapse images of Brn2-GAVPO ES cells exposed to sustained blue light induction of Brn2 for ~50 hours. Frames are every 7 minutes for approx 50 hours.

Figure SI 3: ES cells tolerate sub-threshold levels of Brn2 for greater than 24 hours without differentiation, related to Figure 2 **A)** Nanog-GFP, Brn2-RFP distribution for cells held at a “low” induction power 10uW for 24 compared with 48 Hours (Right). Distribution shows that cells can be stably maintained below the Brn2 switching threshold. **B)** Histogram of Nanog-GFP expression for cells at 24 and 48 hours for Brn2<100. **C)** Nanog-GFP and Brn2-RFP distribution for >10,000 cells following 24 hours of 1 hour light pulses spaced by 6 hour intervals for typical 300 uW illumination used elsewhere. Right hand plot shows trace of Brn2 (mean +/- standard deviation) extracted from time-lapse imaging data. Brn2 level reaches a near constant steady state value within 8-10 hours, suggesting that constant below threshold induction of Brn2 does not induce Nanog down-regulation.

Figure SI 4: Fluctuations and regime tuning in two-state switch model, related to Figure 3. **A)** Left, Distribution of Nanog expression levels in a cell population as a function of Brn2 input as derived from a modified version of the mathematical model that accounts for Nanog fluctuations through a phenomenological framework. Right, Conditional distribution of Nanog for a series of increasing Brn2 levels from modified mathematical model (blue to red for increasing Brn2). **B)** Tuning of Nanog half-life modulates filtering properties of circuit. Diagram shows theoretically-predicted response of pluripotency circuit to pulsed Brn2 inputs of varying magnitude (y-axis) and duration (x-axis). The model predicts that the impulse response of the network has two regimes separated by a boundary: one where the circuit can buffer the input, preventing differentiation (blue shading), and another where cells differentiate in response to the pulse input (red shading). Amplitude and duration thresholds (a,d) simply depend upon the Nanog half-life, so that a doubling of the Nanog half-life doubles the Nanog concentration threshold and approximately doubles the duration threshold.

Figure SI 5: MyoD induction induces a graded down-regulation of Nanog, related to Figure 4 **A,B,C)** Nanog-GFP and MyoD-RFP distributions shown for three light induction powers (4,15, and 25uW). Each experiment contained >30,000 cells. For low light powers, MyoD is induced in cells and Nanog-GFP is down-regulated by Nanog adopts intermediate levels not seen in Brn2 induction experiments. **D)** Phase contrast images of MyoD induced ES cells following 3 days of 300uW light exposure. Images

show phenotypic changes in ES cells induced by MyoD. 40um scale bar. **E)** The relative impact of Brn2 and MyoD induction compared as a function of $V \tau$ for fixed $k = 1/200$ as in our model. In our model $V \tau = 1.05$.

SI Movie 3, Related to Figure 5: Pseudo-colored time lapse image sequence for Nanog-GFP (Green) and Brn2-RFP (red). Frames are captured every 15 minutes for approximately 15 hours.

Figure SI 6: Rapid Nanog protein production balances rapid Nanog degradation in unperturbed ES cell, related to Figure 5. **A)** Nanog-GFP cells were treated with proteasome inhibitor to block protein degradation as described in methods. Plot shows the mean and standard deviation of Nanog-GFP levels at 6 time points following proteasome inhibition as measured by FACS. The red line shows a least squares fit to the linear section of the curve. Fits were performed to middle four time points to focus on time points at which a) drug was activate b) macroscopic effects of protein accumulation had not taken place. The y-axis is normalized to the mean GFP level in the unperturbed ES cell population. The slope of the red line is .45 indicating that cells produce 45% of the steady state Nanog-GFP level every hour. **B)** Nanog-GFP distribution at indicated time points following proteasome inhibition as measured by FACS. Data illustrates that the Nanog-GFP distribution moves to the right in presence of proteasome inhibition, supporting the validity of measurement from A.

Movie SI 4, related to Figure 5: Nanog half-life measurement. A GAVPO-Nanog-RFP cell line was generated for optical pulse chase experiment. Cells were exposed to a one hour pulse of blue light and imaged continuously with frames captured every 20 minutes for 900 minutes. Cells activate Nanog-RFP and then Nanog decays rapidly. Data analysis shown in Figure 4.

Figure SI 7: Mathematical modeling and parameter fits for Brn2 dynamic model; Neurod1 is activated only in Nanog-off cells in light pulse experiments, related to Figure 7. **A)** Plot shows that distribution of Nanog and Brn2 following 24 hours of light input performed simultaneously to the pulse experiments in 6A. Experiment confirms ~100 fold Brn2 threshold. **B)** Plot of steady state normalized Brn2 level as a function of light power. Blue points represent the mean Brn2-RFP level in a population of cells exposed to the indicated light power as measured through FACS. Red curve is derived from a least squares fit to a Hill function model (equation 31 in SI, $V_b = 211$, $k_b = 7$). **C)** Brn2 dynamics in response to a constant light input. Blue dots are data derived from ($N > 10$ cells) analysis of time-lapse image series. Red line is a fit to a hill function model (equation 32 in SI, $m = 4$, $k = 3.8$ hours). **D)** Brn2 half-life measurement. Cells were exposed to a one hour pulse of light and Brn2-RFP was measured in $n = 10$ single cells. Single cell trajectories were averaged and log transformed. Plot shows log transformed data (blue dots) and an exponential fit (red line). Half life extracted from fit is 8.22 ± 1.07 hours. **E)** Simulated Nanog and Brn2 trajectories from mathematical model for

above threshold Brn2 induction. Green curve shows simulated Nanog switching from Nanog-on to Nanog-off. Red curve shows simulated Brn2 induction. Compare with Figure 3. **F)** Images of cells from (A) with Dapi, Nanog-GFP, Brn2-RFP and IF staining for Neurod1. 30 minute light pulse induces Brn2 (top left) but does not down-regulate Nanog. Neurod1 is absent in this cell population, consistent with scatter plots. Five hour light pulse deactivates Nanog and activates Neurod1 in a small sub-population of cells. 24 hour light activation down-regulates Nanog, so that only a small fraction of cells maintain Nanog expression. Neurod1 and Brn2 are active in a large population of cells, and Neurod1 and Nanog are mutually exclusive as shown in color-combined image of Nanog and Neurod1. **G)** Scatter plots of cells stained for Neurod1 exposed to pulses of high light power (300uW) for three different durations (30 minutes, 5 hours, and 24 hours). Plots show that Neurod1 is inactive following a 30 minute light pulse, consistent with the cell population remaining in the Nanog-on state. At 5 hours, a small number of cells activate Neurod1, and Neurod1 is significantly activated for the 24 hour pulse.

Table SI 1: Oligonucleotide sequences used for Nanog-GFP cell line construction, related to Figure 1. Table lists sequences of key DNA and sgRNA constructs used for homologous arm generating and Cas9 mediated insertion of GFP into the Nanog locus.

Supplemental Experimental Procedures:

mESC culture conditions: E14 mouse ES cells were routinely passaged on gelatin coated tissue culture plates, in N2B27 media supplemented with LIF+2i. Optogenetic stem cell lines were maintained in the dark and passaged under red illumination (650 nm wavelength LED) for routine cell culture. Cells were routinely imaged in 24 well imaging plates (Ibidi, 82406).

N2B27 Media (250 ml): 118 ml DMEM/F12 + GlutaMAX (Invitrogen, 10565-018), 120 ml Neurobasal (Invitrogen, 21103-049), 1.25 ml NEAA (Invitrogen, 11140-050), 1.25 ml Sodium Pyruvate (Invitrogen, 11360-070), 1.25 ml GlutaMAX (Invitrogen, 35050-061), 1.25 ml N2 (Invitrogen, 17502-048), 2.5 ml B27 - Vitamin A (Invitrogen, 12587-010), 166 µl BSA (7.5% stock, 50µg/ml) (Gemini, 700-110), 250 µl 2-ME (100 mM 1,000x stock in PBS) (Sigma, M3148-25ML).

2i Media (250 ml). 250 mL N2B27 media, 250 uL LIF (10^6 U 1,000x stock) (Millipore, ESG1107), 75 uL CHIR (10 mM 3,333x stock in DMSO) (Stemgent, 04-0004), 25 uL PD0325901 (10 mM 10,000x stock in DMSO) (Stemgent, 04-0006), Working concentrations: LIF 1000 units/ml, CHIR99021 3 µM, PD0325901 1 µM.

Dual allele Nanog-eGFP dual allele knock-in reporter construction:

The Nanog-GFP knock-in cell line was generated from E14 mouse embryonic stem cells (gift from Chong Park) through Cas9 mediated homologous recombination of eGFP into the C terminus of the endogenous Nanog gene (Figure S2).

Production of sgRNA and DNA donor

The sgRNA expression vector was linearized by a BstXI and XhoI digest and gel purification. The sgRNA sequence was added in the sgRNA primer F (Table S1). The sgRNA was amplified by PCR—with primers sgRNA F and sgRNA R (Table S1). The sgRNA product was digested with BstXI and XhoI, gel purified and ligated to the linearized vector.

The Nanog-GS linker-eGFP vector was assembled with three fragments (5' homologous arm of Nanog, GS linker-eGFP and 3' homologous arm of Nanog) and a vector backbone by using Gibson Assembly Master Mix (New England Biolabs). The 5' homologous arm was amplified by PCR with primers 5'HR F and 5'HR R (Table S1) from genomic DNA of mES cells. The 3' homologous arm was amplified using the same method. The GS linker was added to the eGFP coding region by PCR amplification using primers eGFP F and eGFP R (Table S1). The backbone vector was digested with PmeI and ZraI. The three fragments and the backbone vector were gel purified. The overlapping 5' and 3' arms were added to the backbone vector by PCR amplification with primers vector F and vector R (Table S1). The backbone vector and three fragments were assembled into the Nanog-GS linker-eGFP vector.

Electroporation and clonal mES cell lines

2.5 µg pX330-Cas9, 2.5 µg sgRNA and 15 µg Nanog-GS linker-eGFP donor DNA in 100 µL Nucleofector solution (Lonza) were electroporated into 1×10^6 E14 mES cells using program A-030. After 3 days in culture, sorted single eGFP positive cells were seeded in a 96-well plate with one cell per well. Monoallelic and Biallelic targeting was verified by PCR (Figure S2, Table S1)

Light inducible GAVPO-Brn2 cell line: Optogenetic induction of Brn2 in E14 mES cells was accomplished using the GAVPO blue-light activate-able transcription factor via two PiggyBac vector constructs. The first construct contains the GAVPO gene driven by the eF1alpha promoter with puromycin resistance. The second vector contains Brn2 fused to TAGRFPT2 driven by 5 copies of the GAL4 UAS sequence (pG5) with hygromycin resistance.

To generate the pG5-Brn2 PiggyBac vector, the pG5 promoter region from the Promega vector pG5luc was removed and cloned into a PiggyBac ready vector (DNA 2.0, pJ549) with a hygromycin resistance cassette. Base pairs 1-225, including poly(A)-5XGAL4-TATA (prior to the luc gene), were used to replace the EF1alpha promoter in pJ549 (DNA 2.0). The Brn2 gene was codon optimized for mouse expression and tagged with TAGRFPT2 separated by a glycine serine linker (GGGSGGGSGGGS).

The GAVPO cDNA was synthesized and placed on a PiggyBac plasmid under the control of the EF1alpha promoter (pJ549) with a puromycin resistance cassette. GAVPO and Brn2 constructs were generated by DNA 2.0. Light dependent induction of Brn2-RFP was verified by microscopy and FACS in a blank E14 cell line prior to generating the Nanog-GFP construct.

Biallelic Clone E14N14 was selected from the Nanog-GFP targeting and verified for dual allele tagging (Figure SI 2). The cell line was then transfected serially with Lipofectamine 2000 to introduce Brn2-pG5 and Efla-GAVPO into the cells. Cells were first transfected with the GAVPO construct and selected with puromycin at 1µg/ml for a week. Cells were next transfected with the Brn2-pG5 and selected with dual hygromycin at 30µg/ml and puromycin for one week. Dual antibiotic selection was required to generate a dual eflalpha-GAVPO/pG5-Brn2 ES cell line.

Light inducible GAVPO-UAS-Oct4 and GAVPO UAS-Myod cell lines: The cell lines used in Figure 5 for Oct4 and MyoD induction were generated with exactly the same procedure as the Brn2 line. For these constructs, Brn2 was replaced by codon optimized cDNA for Oct4 or MyoD.

Live-dead cell staining: For FACS quantification of dead cells, 7AAD dead cell stain from Invitrogen was used (A1319). Cells were prepared and dye diluted per manufacturer

instructions. Cells were induced with Brn2-RFP at 300 uW and collected at 0,24, and 48 Hours. 7AAD was measured in >30000 by FACS. Dead cell fraction was quantified by gating on the second peak in the 7AAD distribution. For imaging, the Invitrogen Live/Dead fixable blue dye kit was used (L34961) to stain cells at 48 H post light induction. To validate the assay, cells were exposed to a high light power 1.2mW for 3 days yielding a large number of dead cells that were clearly visible upon staining with the dye.

Microscopy: All imaging experiments were performed with a Nikon Ti-E Microscope with Hamamatsu Flash 4.0 camera, a Sutter Lambda XL lamp, and a Sutter Emission wheel. The Scope was controlled by Nikon Elements software NIS-Elements 4.2 (Build 982). Time-lapse imaging experiments were performed with an in Vivo Scientific incubator and CO2 control Plan Fluor 40x/0.75 (DIC N2 / 40X I) 164nm/pixel Plan Apo 20x/0.75 (DIC N2 / 20X) 327nm/pixel. Standard GFP, RFP, and Cy5 filter sets were used in IF and GFP/RFP imaging experiments. For immunofluorescence experiments, cell nuclei were segmented using Cell Profiler.

For time-lapse imaging, single cell nuclei were tracked using computer assisted manual tracking in Fiji. In all cases, single cell trajectories were extracted from raw image sequences. The mean fluorescent intensity was extracted in a cell nuclei and the local background was subtracted from this value for each data point. Single cell trajectories were smoothed by calculating a windowed average across frames representing one hour of time (4 frames for 15 minute time points). Plots in Figure 5 represent an average of smoothed single cell trajectories. All data analysis was performed in Mathematica and Matlab.

LED induction of Brn2 via Rainbowduino driven LED panel masked with 3D printed tray: An 8x8 LED matrix driven by a Rainbowduino (both from Seedstudio) was used to spatially and temporally control light pulses given to the cells. A custom 3D printed mask was used to ensure optical isolation of individual wells on a 24 well plate. The Rainbowduino driver gives programmatic control over the LEDs in an Arduino-like environment (C), allowing for preset sequences of illumination patterns. Each LED on the matrix is individually addressable. The effective intensity of the LEDs is controllable by modulating the current delivered to each LED. A dispersive element was necessary to ensure uniform illumination across an entire well: a Kim-wipe was used for our purposes. The LED power was calibrated prior to the experiment specifically using a power meter. Control experiments were performed to ensure isolation of individual wells. Fixed duration pulse experiments were performed in individual wells. For pulse time series experiments (Figure 7A, Figure S1), pulses were shifted in time to allow the population response to be interrogated at different time points relative to pulse initiation (Figure 7A).

Optical induction experiments were performed in a standard tissue culture incubator at 37 C and 95% humidity, 5% CO2. Experiments were performed in 10cm plates or in 24 well

plates from Ibidi. Standard Ibidi plates are made of black plastic and optically insulate individual wells for microscopy.

Immunofluorescence: Cells were fixed with 4% PFA, washed with PBS and blocked using standard methods. The following primary anti-bodies and Alexa 647 conjugated secondary anti-bodies were used (1:1000): Anti-beta-tubulin III (Tuji, 1:1000; Covance), Neurod1 (1:300; Santa Cruz Biotechnology sc-1084), Nanog (1:500; ReproCell RCAB0002P-F), Oct4 (1:300; Stemgent 09-0023)

RNA-seq:

RNA-seq experiments were performed in a similar fashion to the other optical induction experiments in the paper. Cells were exposed to 300uW blue light in an Ibidi 24 well plate and samples collected at indicated time points. We note that RNA-seq experiments were performed on the base E14 cell line with the light inducible Brn2 construct prior to the introduction of the integrated Nanog-GFP reporter.

RNA extraction

Total RNA was isolated by using the RNeasy Mini Kit (Qiagen) and treated with Rnasin Plus (Promega). Samples were quality controlled with the NanoDrop ND-1000 (Thermo) and the RNA 6000 Nano Reagents I Kit on the Bioanalyzer 2100 (Agilent).

RNA library preparation

500 ng of total RNA per sample was used to generate multiplexed mRNA-Seq libraries with the SENSE prep kit for Illumina (Lexogen). Samples were quality controlled and multiplexed with the High Sensitivity DNA Reagents Kit on the Bioanalyzer 2100 (Agilent), the Qubit dsDNA HS Assay Kit (Invitrogen) and the SYBR FAST Universal qPCR Kit (KAPA Biosystems). Multiplexed libraries were sequenced on the HiSeq (Illumina) using 150 base pair, single end reads or on the MiSeq (Illumina) using 50 base pair, single-end reads.

RNA-seq Data Analysis

Pass filter reads were de-multiplexed using the MiSeq (Illumina). Base pairs were removed from the 3' and 5' end of all reads where less than 75% of the base pairs showed a Sanger quality below 33 using FastXTrimmer. Individual reads with a quality score below 30 were removed from analysis using Fastq Quality Filter. Reads were aligned to the mm9 mouse transcriptome using bowtie2. Genes with fewer than 10 total reads were removed from analysis.

Gene expression programs were defined by performing non-negative matrix factorization (NNMF) across the temporal time course dataset with a dimensionality of 4. The NNMF dimension was set by first performing PCA on the datasets and defining the number of eigenvalues required to capture 90% of variance. NNMF parts were defined by selecting genes with part coefficient ~~was~~ more than two standard deviations above the mean

coefficient value in the part. Then, GO terms were associated with NMF parts using the hyper-geometric test. Top five pathways by p-value are shown in the Figure 1M. To confirm NMF results, we also examined the correlation matrix of all genes that vary more than two fold over the time course of the experiment (maximum over minimum value is great than 2). A sampled portion of the correlation matrix is shown in Figure 1. The matrix has been clustered and shows the existence of two block gene expression programs.

FACS:

Cells were dissociated into single cell suspension using Accutase (Millipore, SCR005). Suspended cells were fixed for 15 minutes in 4% paraformaldehyde and ~~then~~ washed in PBS. FACS was performed on the LSRII. RFP and GFP were detected using LSRII filters mCherry and FITC. FlowJo X software was used to eliminate debris measurements from the population of cells through forward and side scatter gating.

FACS data analysis: Nanog and Brn2 level were normalized consistently in all FACS experiments. Nanog was normalized to the mean GFP intensity in the undifferentiated mESC population. Brn2 was normalized to the background RFP level in uninduced cells. Fitting of Nanog/Brn2 and Nanog distribution functions is described in the Supporting Information. All FACS analysis was performed in Mathematica and Matlab following gating in FlowJo. The functions lsqcurvefit.m and nlinfit.m were used to fit Nanog-GFP distributions to the Gaussian mixture model as described in the Supporting Information.

For the plot in Figure 2A, FACS data across 9 light powers (4,7,15,25,45,75,100,200,300 μ W) and two experimental replicates were pooled into a single data set with \sim 268,000 data points. The Brn2/Nanog steady state distribution was constructed by sampling 8,000 points uniformly at random from each of 28 Brn2 bins spaced uniformly on a Log10 scale between Brn2 = [0,1000]. The smooth probability distribution function in Figure 2A was constructed using a smooth kernel density estimate of the 2D histogram generated from the raw binned Nanog-GFP FACS data.

The Nanog-GFP histograms within each of the Brn2 bins was also extracted and fit to a Gaussian mixture model as described in the Supporting Information.

Nanog Production rate measurement: 5 μ M of proteasome inhibition Mg132 was added to 5 different populations of E14N14 Nanog-GFP tagged cells in 2i media. Following Mg132 addition, the cells, were fixed in single cell suspension every 30 minutes in preparation for FACS, rendering six time-points: 0 hr, 0.5 hr, 1 hr, 1.5 hr, 2 hr, and 2.5 hr. Using flow cytometer LSRII, GFP-tagged Nanog was measured at each timepoint. After removing background noise, as measured by GFP from blank ES cells, the mean GFP level was calculated at each time-point and normalized to the 0hr Nanog-GFP intensity. The normalized mean intensity at each time point was fit to a linear model using least squares fit in Mathematica. The fit was performed on four time points (0.5 hr, 1 hr, 1.5 hr, 2 hr) to approximate the linear response regime during which the drug is active but complex regulatory processes induced by global increases in protein levels have not yet occurred. The slope of response corresponds to the basal normalized

production rate of Nanog protein in ES cells. The slope represents the fraction of the steady state Nanog pool that is regenerated each hour.

Nanog/Brn2 life-time measurement: A GAVPO inducible Nanog-RFP vector was constructed by replacing Brn2 in pG5-Brn2 vector with codon optimized cDNA coding for Nanog, so that the glycine serine linker and the TAGRFPT were retained. The Nanog-RFP construct was integrated into a blank E14 ES cell line with stable expression of GAVPO under control of the eF1alpha promoter (without Nanog-GFP tag).

To measure the degradation rate of Nanog in ES cells, cells were exposed to a one-hour pulse of blue light in 2i media. Cells were then imaged at 20 time intervals. Individual cells were tracked with computer assisted tracking and the Nanog level estimated using average pixel intensity minus background. Single cell trajectories were log transformed and fit to a linear model using least squares to extract the Nanog degradation rate. The histogram in Figure 4 shows the half-life as calculated from ~50 single cell trajectories. Half-life is reported as mean and standard deviation $\text{Ln}[2]/\tau$ where tau is the decay time constant extracted from the fit.

Standard Neural differentiation experiment in SI: 46C Sox1-GFP mES cells were differentiated into the neural lineage—by inhibition of Fgf , Nodal, and BMP signaling. PD0325901 1 μM (Mek inhibitor), A8301 (Nodal/Tgfb inhibitor, 1 μM), LDN193189 (Bmp antagonist, 0.5 μM) for Sox1+. Cells were harvested at indicated time points (0, 4, 9, 11 days, Figure S4). RNA-seq analysis performed as described above.

Mathematical modeling and numerical integration: The mathematical model is described in detail in the supporting information. Numerical integration of the model was performed using NDSolve in Mathematica.

Supporting Information: Mathematical Model

In the experimental section of the main text, we study the quantitative response of the pluripotency network to the temporally controlled induction of Brn2 and make three experimental observations: (i) Brn2 induction can switch the cell (discretely) from a Nanog-on to a Nanog-off state. (ii) Switching occurs at a threshold level of Brn2 that is 100-fold Brn2 induction over background with a 4 hour relaxation time. (iii) Due to the dynamics of the switch and Nanog relaxation, the pluripotency network can reject transient pulses of Brn2 that are below sharp amplitude and duration thresholds. In this way, the stem cell uses the relaxation dynamics of a two-state switch to classify a Brn2 input as a fluctuation or a command. The dynamics of the network rejects fluctuations while allowing rapid differentiation in response to above threshold inputs. We call the network an impulse filter due to its ability to reject pulsatile inputs of defined amplitude and duration.

Here, we develop a simple mathematical model of the pluripotency circuit, and its interaction with Brn2, and explore how these three behaviors might arise from the underlying biochemical interactions in the system. Our model is a system of two coupled ODEs:

$$\frac{dN}{dt} = f_1(N, B) \quad (1)$$

$$\frac{dB}{dt} = f_2(L), \quad (2)$$

which describe the dynamics of Nanog, N , and Brn2, B . The function f_1 models the core pluripotency circuit and its interaction with Brn2; f_2 models the dynamics of Brn2 as a function of the light input into the system, L . Below, we develop functional forms for f_1, f_2 based upon known biochemical features of the circuit and analysis of our data.

Model of the pluripotency circuit as a one component auto-regulatory loop

The pluripotency network is composed of a set of transcription factors (including Nanog, Oct4, and Sox2 [Figure 1A]). The factors bind to form a protein complex that, in turn, activates the components of the circuit, so that Nanog, Oct4, and Sox2 regulate their own expression levels through an auto-regulatory positive feedback loop. Biochemical studies have shown that Nanog, Oct4, and Sox2 form a complex at the Oct4 promoter that drives Oct4 expression (Chen,2008;Jaenisch, 2008) . While biochemical studies have verified the core auto-regulatory topology of the circuit, the detailed on and off rates for complex formation and promoter binding have not been characterized. Therefore, we develop a coarse grained model of the circuit that minimizes the number of parameters and allows direct comparison with our quantitative data.

Specifically, we reduce the number of degrees of freedom in the system by modeling the three component pluripotency circuit as a single element. Generally, Nanog expression

will depend upon the concentration of the Nanog-Oct4-Sox2 (NOS) protein complex:

$$\frac{dN}{dt} = V \frac{[\text{N-O-S}]^m}{k^m + [\text{N-O-S}]^m} - \frac{N}{\tau}, \quad (3)$$

where $[\text{N-O-S}]$ is the Nanog-Oct4-Sox2 protein complex concentration. The Hill function with threshold k , maximum production rate V , and promoter cooperativity m , models the influence of the NOS complex on Nanog production. The N/τ term accounts for simple first order degradation.

If we consider complex formation to be at equilibrium, and Oct4, Sox2, and Nanog to experience symmetric regulation, then:

$$[\text{N-O-S}] \propto [\text{Nanog}]. \quad (4)$$

While sacrificing biochemical complexity, this simplification allows us to develop a one-dimensional model of the underlying regulatory circuit with a small number of free parameters that we can constrain with our data.

We can construct a simple 1D model of this positive feedback loop by considering an auto-regulatory loop generated by a single component, Nanog:

$$\frac{dN}{dt} = V \frac{N^m}{k^m + N^m} - \frac{N}{\tau}, \quad (5)$$

where we have substituted $[\text{N-O-S}] \rightarrow N$, and Nanog production depends on the current concentration of Nanog accounting for the auto-regulatory positive feedback in the pluripotency circuit.

Brn2 Destabilization of Circuit

Next, we consider the interaction of this positive feedback loop with Brn2 and show that Brn2 can induce a transition between on/off Nanog states by destabilizing the positive feedback loop.

Brn2 has been shown to bind Sox2 and to sequester it from Oct4, inactivating the Oct4-Sox2 protein dimer (Lodato, 2013), so that



Specifically, the rate of dimer formation is determined by kinetic on-off rates, but Nanog protein levels are changing on transcriptional time scales (hours), which are much slower than timescales of protein binding and unbinding (seconds). Therefore, protein association/disassociation approximately equilibrates for any transient Nanog copy number.

At equilibrium, the concentration of the inactive Brn2-Sox2 complex is proportional to both the amount of free Brn2 and Sox2.

$$[\text{Brn2-Sox2}] = K_B [\text{Brn2}] [\text{Sox2}], \quad (7)$$

where K_B is an equilibrium binding constant. Now,

$$\text{Sox2}_{\text{total}} = [\text{Sox2}] + [\text{Brn2-Sox2}] \quad (8)$$

$$\text{Sox2}_{\text{total}} = [\text{Sox2}] + K_B[\text{Brn2}][\text{Sox2}] \quad (9)$$

$$[\text{Sox2}] = \frac{[\text{Sox2}_{\text{total}}]}{1 + K_B[\text{Brn2}]} \quad (10)$$

$$[\text{Sox2}] = \frac{[\text{Sox2}_{\text{total}}]}{\gamma} \quad (11)$$

where $\gamma = 1 + K_B[\text{Brn2}]$. $[\text{Brn2}]$ is a time-varying quantity under external control through the optogenetic system. Thus, the free concentration of Sox2 that is available to interact with Nanog and Oct4 is effectively decreased by Brn2.

This change in $[\text{Sox2}]$ will decrease the concentration of the Nanog-Oct4-Sox2 complex:

$$[\text{Nanog-Oct4-Sox2}] \sim [\text{Nanog}][\text{Oct4}][\text{Sox2}] \quad (12)$$

$$[\text{Nanog-Oct4-Sox2}] \sim [\text{Nanog}][\text{Oct4}] \frac{[\text{Sox2}_{\text{total}}]}{\gamma}, \quad (13)$$

so we can model Brn2 as decreasing the effective concentration of the pluripotency complex. Recalling equations (3) and (5), we scale the concentration of the [N-O-S] complex, represented by N , by γ , so the scaled equations become:

$$\frac{dN}{dt} = V \frac{\left(\frac{N}{\gamma}\right)^m}{k^m + \left(\frac{N}{\gamma}\right)^m} - \frac{N}{\tau} \quad (14)$$

$$\frac{dN}{dt} = V \frac{N^m}{(\gamma k)^m + N^m} - \frac{N}{\tau} \quad (15)$$

$$\frac{dN}{dt} = V \frac{N^m}{k'^m + N^m} - \frac{N}{\tau}. \quad (16)$$

Note that $k' = \gamma k = k(1 + K_B[\text{Brn2}])$, so that the threshold for the positive feedback loop now depends upon $[\text{Brn2}]$. We can interpret this influence of Brn2 as increasing the threshold for Nanog promoter activation. In [Figure 4B], this effect is seen in the rightward shift of the Nanog production Hill function with increasing $[\text{Brn2}]$.

Equation (16) is our model of the pluripotency circuit and its behavior in response to Brn2 induction.

Switching at Steady State

First, we analyze the steady-state behavior of (16) and demonstrate that Brn2 drives dose-dependent, steady-state switching.

At steady state, Nanog concentration, $\frac{dN}{dt} = 0$, and for a mildly cooperative Nanog promoter ($m = 2$), we find:

$$N = 0, \frac{\tau}{2} \left(V \pm \sqrt{V^2 - 4 \frac{k'^2}{\tau^2}} \right), \quad (17)$$

and the system has one or three real, positive fixed points or steady states depending upon the sign of $D \equiv (V^2 - 4k'^2/\tau^2)$. When $D > 0$, the system has three steady states; straightforward analysis shows that low (0) and high (+) steady states are always stable, and the middle (−) steady state is always unstable. We also refer to this unstable steady state as N^* .

We interpret the $N = 0$ fixed point as the Nanog-off fixed point, N_{off} , and interpret the $N = \frac{\tau}{2} (V + \sqrt{V^2 - 4 \frac{k'^2}{\tau^2}})$ as the Nanog-on fixed point, N_{on} .

The existence of the Nanog-on fixed point depends upon $k' = k(1 + K_B[\text{Brn2}])$:

$$V^2 - \frac{4k'^2}{\tau^2} \geq 0 \quad (18)$$

Increasing k' , which is a function of [Brn2], destroys the fixed point.

This relation can be used to determine a threshold level of [Brn2] at which the Nanog-on stable fixed point disappears. From (18),

$$k' = \frac{V\tau}{2} \quad (19)$$

$$k(1 + K_B B) = \frac{V\tau}{2} \quad (20)$$

$$B^* = \frac{1}{K_B} \left(\frac{V\tau}{2k} - 1 \right) \quad (21)$$

where B^* is the [Brn2] threshold. When $B^* > \frac{V\tau}{2k} - 1$, Brn2 has pushed the system across a bifurcation where the Nanog-on fixed point vanishes. Dynamically the system must relax to the Nanog-off fixed point.

Energy Landscape picture

We can visualize the global behavior of the system for increasing [Brn2] by thinking of (16) as emerging due to [Nanog] dynamics on a potential landscape:

$$\frac{dN}{dt} = -\mu \frac{dU}{dN} \quad (22)$$

$$U(N, B) = -k'V \arctan \frac{N}{k'} + VN - \frac{N^2}{2\tau}, \quad (23)$$

where U is an effective potential function, and μ is a proportionality constant analogous to mobility. The local minima of H (where $\frac{dU}{dN} = 0$) correspond to fixed points. We plot $U(N, B)$ for increasing [Brn2] in Figure 3E for sample parameters $V = 14, k = 11, \tau =$

1.85 for convenient plotting purposes. As [Brn2] increases, the minimum of U shift upwards destabilizing the Nanog-on state.

This energy landscape picture allows us to naturally incorporate fluctuations into the model. This equation:

$$\frac{dN}{dt} = -\mu \frac{dU}{dN} + \eta(t) \quad (24)$$

$$U(N, B) = -k'V \arctan \frac{N}{k'} + VN - \frac{N^2}{2\tau}, \quad (25)$$

has the same form as the Langevin dynamics for a particle moving in a potential well of shape U where $\eta(t)$ is a random term modeling fluctuations in Nanog. Therefore, the energy landscape allows a natural extension of the model to model a distribution of cells (particles) through the Fokker-Plank formalism (manuscript in preparation). Briefly, $U(N, B)$ can be used to directly generate a model of the distribution of Nanog expression levels, $P(N, t)$, in a differentiating cell population over time (in response to Brn2 input) where the population is subject to fluctuations. For simplicity, we consider $\langle \eta(t)\eta(t') \rangle \sim \delta(t-t')$ and generate the Smoluchowski equation corresponding to :

$$\frac{dP(N, t)}{dt} = \frac{1}{\zeta} \frac{d}{dN} (U'(N, B) P(N, t)) + \frac{T}{\zeta} \frac{d^2}{dN^2} P(N, t), \quad (26)$$

where ζ and T are phenomenological 'drag' and 'temperature' terms respectively. In SI Figure 4A we plot the Nanog distribution function at steady state, $\frac{dP(N, t)}{dt} = 0$ where $P(N, t) = \exp(-U(N, B)/T)/Z$ at a value of $T = 50$ and Z is a normalization factor to normalize probability distributions to 1. The distribution of Nanog as a function of Brn2 induction is qualitatively similar to Figure 2A (manuscript in preparation).

Switching Dynamics

When the Nanog-on fixed point is destroyed, Nanog begins to switch (or "relax") to the $N = 0$ steady state. We can ask how long it takes Nanog to relax to the Nanog-off state for a constant [Brn2] input. In general, the switching time will depend upon the competition between Nanog degradation and residual Nanog production, and hence it will depend upon [Brn2]. However, we can approximate the relaxation time by considering a system in which the Nanog production rate has become 0. In this approximation, the system relaxes exponentially:

$$\frac{dN}{dt} = -\frac{N}{\tau} \quad (27)$$

$$N(t) = N(t=0) e^{-\frac{t}{\tau}} \quad (28)$$

$$N(t) = N_{\text{on}} e^{-\frac{t}{\tau}}, \quad (29)$$

where N_{on} is the level of Nanog in the Nanog-on state, and the relaxation time is set by τ , the Nanog lifetime.

Experimentally, our measured relaxation time will be influenced by residual production of Nanog and therefore will always be *longer*, than the estimated τ . Therefore, the measured relaxation time τ_m provides an upper bound on τ in the model.

In summary, the simple mathematical model provides a mechanism for circuit switching and connects the relaxation time of the circuit to the intrinsic degradation rate of the Nanog protein τ .

Competitive binding vs global inhibitor

In this section, we compare the response of the regulatory network to factors that decrease V (modeling global inhibition) with factors that interact with the network through competitive binding which scales k . Interestingly, these two modes of interaction lead to distinct Nanog behavior. For the unperturbed model, the Nanog-on fixed point occurs at:

$$N_{\text{ss}} = \frac{V'\tau}{2} \left(1 + \sqrt{1 - 4 \frac{k'^2}{(V'\tau)^2}} \right), \quad (30)$$

where we have taken k' and V' to be adjustable parameters. We notice immediately that k' and V' distinctly couple to the Nanog-on steady state. While the Nanog-on state linearly scales (increasing or decreasing) with changes in V , increases in k' modeling competitive binding couple to the steady state in a more subtly way. We want to understand how small increases in k' modeling low levels of a competitive binding factor (such as Brn2) impact the steady state as compared to low levels of induction of a global inhibitory factor which we model as decreasing V' to model global inhibition by MyoD.

To do so, we calculate:

$$\frac{dN_{\text{ss}}}{dk'} = - \frac{2k'}{\sqrt{-4k'^2 + (\tau V')^2}} \quad (31)$$

$$\frac{dN_{\text{ss}}}{dV'} = .5 \left(\tau + \frac{\tau^2 V'}{\sqrt{-4k'^2 + (\tau V')^2}} \right). \quad (32)$$

$$r = \frac{\left| \frac{dN_{\text{ss}}}{dV'} \right|}{\left| \frac{dN_{\text{ss}}}{dk'} \right|} = \frac{\left| \frac{dN_{\text{ss}}}{d\text{MyoD}} \right|}{\left| \frac{dN_{\text{ss}}}{d\text{Brn2}} \right|} \quad (33)$$

Due to the presence of the constant term, τ , in $\frac{dN}{dV'}$, as well as the relative magnitudes of $V\tau$ and k' in our model prior to Brn2 or MyoD induction, $\left| \frac{dN_{\text{ss}}}{dV'} \right| \gg \left| \frac{dN_{\text{ss}}}{dk'} \right|$. For the values of V , τ , and k used in our model the ratio, r , is ≈ 100 . In the SI Figure we show the magnitude of r as a function of the product $V\tau$ to provide evidence that this factor is large in our parameter regime.

Kinetic filtering: rejecting Brn2 pulses based upon duration

Now, we consider the response of the network to a pulsatile [Brn2] input, an input that is above threshold $[\text{Brn2}] > B^*$ for a fixed duration d , but that returns to $[\text{Brn2}] = 0$ for $t > d$. We ask whether Nanog remains "on" or switches "off" following this Brn2 "pulse" and derive an approximate minimum value of d for network switching.

As in the relaxation dynamics argument, when [Brn2] crosses the switching threshold, Nanog begins transitioning from the Nanog-on to the Nanog-off state (Figure 4). The Nanog-on and Nanog-off states are separated by an unstable fixed point (referred to as N^* when $[\text{Brn2}] = 0$). If [Nanog] has fallen past the unstable fixed point ($N(d) < N^*$), then Nanog will relax to the Nanog-off steady state when [Brn2] returns to 0. Alternately, if $N(d) > N^*$, then Nanog will remain in the Nanog-on state following the pulse.

To estimate the critical pulse duration d^* , as above, we model [Nanog] as decaying exponentially when Brn2 is above threshold:

$$N(d) = N_{\text{on}} e^{-\frac{d}{\tau}} \quad (34)$$

$$N^* = N_{\text{on}} e^{-\frac{d^*}{\tau}}, \quad (35)$$

so that $d^* = \tau \log(N_{\text{on}}/N^*)$ is the critical pulse duration. Since $(N_{\text{on}}/N^*) > 1$ (the unstable fixed point occurs at a Nanog concentration less than the Nanog-on concentration), $d^* > \tau$ so that the minimum pulse duration is lower bounded by τ the intrinsic Nanog life-time.

This argument makes several key simplifications. First, Nanog relaxation is not strictly exponential because the Nanog production rate does not go identically to 0 when Brn2 is present. Second, for simplicity we have considered the case of Brn2 switching from on to off i.e. to 0. More generally, Brn2 can simply drop below the switching threshold, and the position of the unstable fixed point at that new Brn2 level (unstable point shown in Figure 4) will determine the final state of the circuit.

Steady-state response to perturbations

To explore the response of the circuit to perturbations near the Nanog-on steady state, we can consider a linearized steady state model of (16):

$$\frac{dN}{dt} = V - \frac{N}{\tau}. \quad (36)$$

$$(37)$$

In this model, small increases or decreases in [Nanog] relax exponentially to steady state like

$$\tilde{N}(t) = \tilde{N}(0) e^{-\frac{t}{\tau}}, \quad (38)$$

where $\tilde{N} = N - N_{ss}$ measures the deviation of Nanog from its steady state value, and τ , the Nanog lifetime, sets the time scale over which perturbations are damped by the system; and $\tilde{N}(0)$ is the magnitude of the perturbation. In this way, the relaxation of perturbations and the relaxation of the system to the Nanog-off steady state following Brn2 induction are intimately connected.

Fitting the Model to Data

In this section, we fix the underlying parameters in the the model using experimental data. The mathematical model has four free parameters: k , K_B , V , and τ . We consider [Brn2] in units of K_B and fix the remaining free parameters. We eliminate V by scaling the Nanog-on steady state to 1, determine k using the [Brn2] threshold measurement, and fix τ via the direct measurement of the Nanog lifetime.

First, we scale the Nanog-on steady state to one by setting:

$$1 = \frac{\tau}{2} \left(V + \sqrt{V^2 - 4 \frac{k'^2}{\tau^2}} \right), \quad (39)$$

$k' \rightarrow k$ since [Brn2] = 0, so that

$$V = \frac{(1 + k^2)}{\tau}. \quad (40)$$

This equation fixes V in terms of k and τ .

Next, we use the measured threshold for [Brn2] switching, B^* , to fix k by solving (21) for k :

$$k = 1 + B^* - \sqrt{B^*(2 + B^*)} \quad (41)$$

The parameter τ is fixed by a direct measurement Figure SI 7D, and B^* is set by the Brn2 threshold. With these free parameters fixed, we have fully parameterized the auto-regulatory model.

We have $\tau = 182$ min (half life: $\tau \log(2) = 2.1$ hours), $k = 1/200$ (unit-less due to scaling), and $V = .0058 \text{ min}^{-1}$ where Nanog is normalized to the Nanog-on steady state.

Parameterizing Brn2 Activation Model

Brn2 activation depends upon exogenous light inputs and is independent of Nanog. We take a phenomenological approach to modeling Brn2 dynamics based upon fits to time-course activation and steady-state Brn2 data.

We model Brn2 dynamics as being controlled by production and degradation terms:

$$\frac{dB}{dt} = g(L, t) - \frac{B}{\tau_b}, \quad (42)$$

where $g(L, t)$ describes the light-power-dependent and time-dependent production of Brn2, and τ_b is the Brn2 life-time.

We decompose $g(L, t)$ into two terms: one accounting for the steady-state activation level and a time dependent term that models the kinetics of activation.

To parameterize the steady-state behavior of Brn2, we collected cell populations following 24 hours of exposure to nine different light powers and fit the dependence of mean [Brn2] on light power to a Hill function with least squares (SI Model Fig 7B):

$$B(L) = V_b \frac{L^m}{k_b + L^m} \quad (43)$$

where L is the light power. [Brn2] has been normalized to the background as in Figures 1-5 of the main paper. k_b is the threshold light power for activation. We found $k_b = 7.0 \text{ uW/cm}^2$, $m = 1$, and $V_b = 211$ (normalized units).

To parametrize Brn2 dynamics, we collected time-lapse images of Brn2 at $L = 300 \text{ uW/cm}^2$, and we fit the activation profile to a Hill function (Figure SI7 C):

$$h(t) = \frac{t^m}{k_t + t^m}, \quad (44)$$

where we determined $m = 4$ and $k_t = 3.8$ hours due to the lag phase in activation that we consistently observed in the curves.

Through optical Brn2 pulse-chase experiments, we determined $\tau_b = 10.4$ hours (half-life: $7.22 \pm .8$ hours, Figure SI7 D):

$$\frac{dB}{dt} = 250 \left(\frac{L}{7 + L} \right) \left(\frac{t^4}{3.8^4 + t^4} \right) - .096B \quad (45)$$

Figure SI7 E shows a sample simulated trace from the model that demonstrates Brn2-dependent Nanog switching.

Modeling the circuit's response to light pulses

To model pulses dynamically, we considered light pulses of a fixed duration d and amplitude a . We set $L = a$ for $t < d$, and $L = 0$ for $t > d$. To determine the steady-state level of Nanog, (16) and (45) were numerically integrated for 24 hours of simulated time.

Data Analysis

In Figure 2, we analyze the conditional distribution of Nanog-GFP vs [Brn2] level by fitting to a Gaussian mixture model. Specifically, we first binned [Brn2] uniformly on a log scale into 12 bins. The bin size was selected to be large enough to generate smooth Nanog-GFP distributions. For each [Brn2] bin, we generated a histogram of Nanog-GFP intensities.

We fit these Nanog-GFP distributions to a gaussian mixture model where:

$$p(N) = \frac{\exp(\frac{-k_L(N-N_L)^2}{2k_B T}) + \exp(\frac{-\Delta E}{k_B T} - \frac{k_R(N-N_R)^2}{2k_B T})}{Z} \quad (46)$$

$$Z = \sqrt{2\pi} \left(\frac{1}{k_L} + \frac{\exp(-\Delta E)}{\sqrt{k_R}} \right). \quad (47)$$

This model describes the distribution of particles in a double-well potential where wells are centered at N_L and N_R . k_L and k_R are spring constants that describe the stiffness of the underlying potential. $k_B T$ is the Boltzmann factor, here set to 1. ΔE is an energy difference between the two wells, and Z is a normalization constant.

Operationally, we fit the conditional [Nanog] distributions in two steps. First, we fit the marginal [Nanog] distribution ([Nanog] distribution over all [Brn2] levels). This fit gave us starting values for N_L and N_R . We use these values as initial conditions in a numerical fit for each of the conditional distributions $P([\text{Nanog}]|[\text{Brn2}])$.

For low [Brn2], $\Delta E < 0$ favors occupation of the Nanog-on steady state (Figure 2D). ΔE increases with [Brn2] (Figure 2D) inducing a tilt in the double-well potential landscape and favoring occupation of the Nanog-off state.

We selected this form for the gaussian mixture model because it has a natural interpretation as a potential well. The form of the underlying potential is:

$$E(N, B) = -k_B T \log(p(N)) \quad (48)$$

$$E = -k_B T \ln \left(\exp \left\{ \frac{-k_L(N - N_L)^2}{2k_B T} \right\} + \exp \left\{ \frac{-\Delta E}{k_B T} - \frac{k_R(N - N_R)^2}{2k_B T} \right\} \right) \quad (49)$$

$$p(N|B) = \exp \left(\frac{-E(N, B)}{k_B T} \right). \quad (50)$$

We have constructed an energy landscape $E([\text{Nanog}], [\text{Brn2}])$ and the distribution of [Nanog] in the cell population is determined by the structure of this landscape. The energy landscape tilts with Brn2 induction leading to a redistribution of the cell population.

$$\frac{dN}{dt} = V \frac{N^m}{k'(\text{Brn2})^m + N^m} - \frac{N}{\tau} \quad (51)$$

$$(52)$$

$$k' \propto \text{Brn2} \quad (53)$$

Note that $k' = \gamma k = k(1 + K_B[\text{Brn2}])$, so that the threshold for the positive feedback loop now depends upon [Brn2]. We can interpret this influence of Brn2 as increasing the threshold for Nanog promoter activation. In [Figure 4B], this effect is seen in the rightward shift of the Nanog production Hill function with increasing [Brn2].